When Black-Box Robot Policies Fail: Online Sensor Diagnosis and Repair with a Transparent Surrogate

Marc Ziegler[1] **Batu Özen**[1] **Sami Mentes**[1] **Thomas Waschulzik**[2] **Alois Knoll**[1]
[1]Technical University of Munich [2]Siemens Mobility
marc.eric.ziegler@tum.de

arXiv:2610.36852v1 [cs.RO] 27 Oct 2026

Abstract: Robot foundation models may generalize across tasks and embodiments, but their actions still depend on sensors that can fail. When the policy is frozen or inaccessible, can an external monitor diagnose and repair corrupted inputs without access to its internals? We test a structured surrogate that separates periodic gait from sensor-dependent corrections to guide input repair around a frozen locomotion policy. On simulated Go2, offline diagnosis raises walking success from 259/640 to 429/640 episodes; online repair reaches 382/640, with no triggers in 64 held-out fault-free episodes. A matched boosted-tree surrogate predicts clean actions similarly well but yields no detected repair improvement over no repair. Separate fits improve walking on Go1 and ANYmal C, although phase-aware gradients perform better. Evidence remains limited to one policy and a partly screened simulated fault suite; robot foundation model and hardware validation remain open.

Keywords: physical AI safety, sensor-fault diagnosis, interpretable surrogates, black-box monitoring, fault-tolerant robot control

1 Introduction

Robot foundation models promise transfer across tasks and embodiments [1, 2], yet their actions depend on reliable sensor observations. When internals are inaccessible, monitors see only inputs and actions. We study the frozen multi-embodiment URMA locomotion policy [3]. On Go2 at $0.5\,\mathrm{m/s}$, a $0.3\,\mathrm{rad/s}$ yaw-gyroscope bias prevents walking in 16/16 episodes. Classical diagnosis uses plant or sensor models [4], whereas gradient attribution and VLA steering require policy access [5, 6, 7, 8]. Runtime guardrails constrain plans [9], while masked training builds sensor robustness into the policy [10]. Unusual sensor readings may nevertheless result from legitimate disturbances.

Prior work distills locomotion into boosted trees or symbolic expressions [11]. Structured controllers and sparse mixtures also expose control structure [12, 13]. Our surrogate separates periodic gait from sensor-dependent corrections, ranks abnormal input contributions, and guides repair. The frozen policy produces every action, so the surrogate never replaces the controller.

We contribute diagnosis and repair without policy gradients, paired offline and online evaluations, and tests on three quadrupeds. This controlled setting motivates external supervision for robot foundation models [14]. Direct validation on those models remains open.

2 Method

Structured action surrogate. Used only for diagnosis, the surrogate predicts 12 joint-action targets u_t at command speed v (Figure 1):

$$u_t = u_{\mathrm{F}}(\varphi_t, v) + \mathrm{clip}_{[-0.15,0.15]}(r_t), \qquad r_{t,j} = b_j(\varphi_t, v) + \sum_i c_{i,t,j}. \tag{1}$$

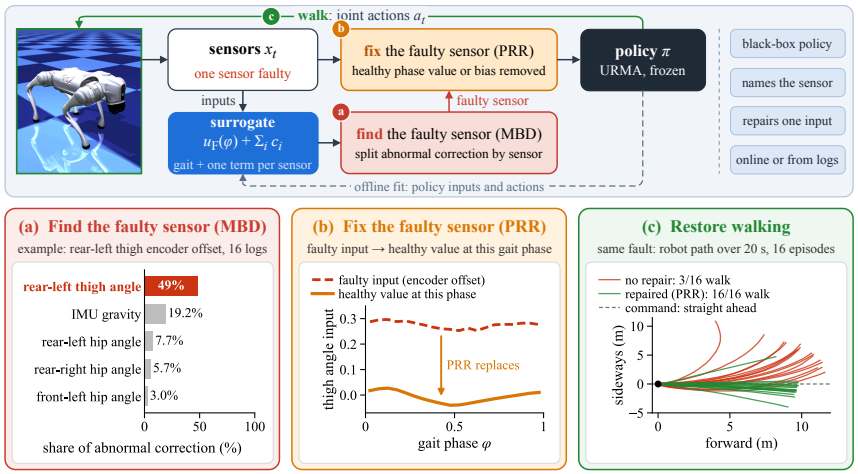

Figure 1: **Method overview: Diagnosis and input repair.** MBD identifies the faulty sensor from the structured surrogate's per-sensor contributions, and PRR repairs its input before the frozen policy acts. For a $+0.3$ rear-left thigh-encoder offset: (a) the sensor explains 49% of the abnormal correction across 16 diagnosis logs; (b) PRR supplies its phase-matched healthy value; and (c) repair removes the sideways drift and raises walking success from 3/16 to 16/16 fresh episodes.

We represent the gait u_F using four Fourier harmonics. Both the gait and correction models are conditioned on the commanded speed v. The correction r_t combines a phase-dependent baseline $b_j(\varphi_t, v)$ with contributions from individual input features. The contribution $c_{i,t,j}$ of standardized input $z_{i,t}$ to joint j is $c_{i,t,j} = z_{i,t}[a_{ij}(v) + a^{\mathrm{s}}_{ij}(v)\sin(2\pi\varphi_t) + a^{\mathrm{c}}_{ij}(v)\cos(2\pi\varphi_t)]$. The 57 inputs describe base motion, gravity, joint states, previous actions, contacts, command, and timing. The baseline and contributions exactly reconstruct the surrogate's correction before clipping.

We collect 64,000 policy state–action pairs at four speeds, fit the gait, then fit the remaining action error by ridge regression. Feedback fitting filters startup and invalid-phase rows and holds out episodes. We also collect 32,000 policy action targets at states reached under alternating policy/surrogate control [15] to broaden feedback training.

Front-left touchdown resets the gait phase. Between touchdowns, the clock advances using its latest period estimate; touchdown intervals of 8–60 steps update this estimate with averaging rate 0.2. Offline fitting and fault-free reference construction use simulator-derived contacts. During diagnosis and repair, phase is computed from the potentially corrupted contact readings visible to the policy.

Diagnosis from abnormal corrections. Mechanism-based diagnosis (MBD) uses the surrogate's additive decomposition to identify which sensor contributions drive abnormal corrections. We discretize gait phase into 20 equal bins (5% of a cycle each); this resolution was fixed before fault evaluation. From fault-free trajectories, we estimate in each bin β the mean and standard deviation of each joint correction, $\bar{r}_j(\beta)$ and $s_j(\beta)$, and the mean contribution of each input, $\bar{c}_{i,j}(\beta)$. At time t, joint j is flagged when its correction deviates from the phase-matched reference by more than two standard deviations: $\mathcal{F} = \{(t,j) : |r_{t,j} - \bar{r}_j(\beta_t)| > 2s_j(\beta_t)\}$. For each sensor unit U, MBD then computes

$$S_U = \sum_{(t,j)\in\mathcal{F}} \sum_{i\in U} \big(c_{i,t,j} - \bar{c}_{i,j}(\beta_t)\big)\,\mathrm{sgn}\big(r_{t,j} - \bar{r}_j(\beta_t)\big). \tag{2}$$

Thus, contributions that push a flagged correction farther in its abnormal direction increase the sensor's score, whereas opposing contributions decrease it. MBD ranks 34 sensor units: the gyroscope, gravity vector, 12 joint positions, 12 joint velocities, four contacts, and four contact ages.

Offline diagnosis aggregates scores across 16 faulty trajectories, excluding the first 25 steps and the final 50 steps before a fall. Although evaluation assumes that a fault is present, MBD abstains when no corrections are flagged.

Baselines. *Phase deviation* measures departure from each sensor's healthy value at the same phase: $|x_i - \bar{x}_i(\beta)|/s_i^x(\beta)$. It averages over channels in each sensor unit and sums over time. A gated variant uses only steps where MBD flags an abnormal correction. *Phase-aware gradients* require policy internals. They compute $(x_i - \bar{x}_i(\beta))^2 \|\partial\pi/\partial x_i\|_2^2/12$ per channel, subtract its healthy phase-conditioned baseline, average over time, and sum across channels in each sensor unit. *GBM–TreeSHAP* uses twelve boosted regressors [16]. Both fits use the same 12,740 clean and 7,827 alternating-control rows, with identical inputs, splits, normalization, nominal gait, residual target, and correction bound. TreeSHAP uses tree-path-dependent expectations [17]. We group its attributions by sensor and apply Eq. (2) with its own anomaly mask. All methods share sensor groups, diagnosis seeds, repair episodes, and PRR.

Input repair and online detection. Phase-referenced repair (PRR) changes only the selected unit U. For a sensor that varies with phase, it supplies the healthy standardized mean, $\hat{z}_{U,t} = \bar{z}_U(\beta_t)$. Otherwise, it estimates and subtracts bias:

$$\hat{z}_{U,t} = z_{U,t} - \hat{b}_{U,t}, \qquad \hat{b}_{U,t} = 0.99\hat{b}_{U,t-1} + 0.01\left[z_{U,t} - \bar{z}_U(\beta_t)\right], \quad \hat{b}_{U,0} = 0. \tag{3}$$

The score $\kappa_U = |U|^{-1} \sum_{i \in U} \mathrm{SD}_\beta[\bar{z}_i(\beta)]$ measures how strongly a sensor normally varies over the gait cycle. If $\kappa_U \geq 0.4$, PRR replaces its reading with the healthy reference for the current phase. Otherwise, it estimates and subtracts an additive bias. We selected the threshold using development data. Contacts and contact ages are replaced with constant nominal values. Repaired values return to policy input units before the next policy call. All repair rules were fixed before evaluation.

Offline MBD diagnoses prior faulty trajectories; repair runs in fresh episodes. Online MBD starts after 25 steps and measures the fraction of flagged joint–time pairs in nonoverlapping 50-step windows at $50\,\mathrm{Hz}$. From the fifth window onward, it triggers when the lower quartile over all completed windows exceeds a calibrated threshold. We calibrate on 128 fault-free episodes in total. Each noise regime's threshold is the maximum of this statistic over its calibration episodes and decision times. Evaluation supplies the true noisy/noiseless regime. At the first trigger, accumulated scores select a sensor; repair starts on the next step and lasts until episode end. Runtime needs no policy weights, gradients, or additional policy calls.

3 Experiments

Protocol. URMA controls Go2 in MuJoCo for 20 seconds at $50\,\mathrm{Hz}$ from randomized starts, commanded at $v = 0.5\,\mathrm{m/s}$. Pushed episodes receive a $250\,\mathrm{N}$ force in a random horizontal direction for 0.2 seconds at six seconds. Survival means completing the episode. Walking also requires mean velocity in each planar axis, after the first two seconds, to be within $\max(0.05\,\mathrm{m/s}, 0.25v)$ of its command. The 37 injected faults comprise 22 main cases and 15 extensions: offsets, stuck readings, drift, dropout, spikes, and contact errors. During method development, we selected 10 main cases based on preliminary MBD performance. We report this development-informed subset separately from the remaining cases. Diagnosis uses 16 trajectories per fault (seeds 2100–2115). Repair uses fresh seeds 2120–2135 on 20 main faults excluding the phase anchor, with/without push: 640 paired episodes per method. Fitting and calibration data are separate from diagnosis and repair data. Diagnosis and repair share healthy references. Contacts are simulated policy inputs, and the fault suite is a constructed stress test, not a sample of hardware failure frequencies. Only online tests assess detection. We report two-sided exact McNemar tests, unadjusted for multiple comparisons, and a bootstrap over the 20 repaired fault types; inference is conditional on this suite.

Diagnosis and repair. MBD identifies 27/37 faults: 8/10 screened main, 9/12 remaining main, and 10/15 extensions. Phase-aware gradients identify 33/37 ($p = 0.11$ versus MBD); phase deviation identifies 8/37 ($p = 2.1 \times 10^{-5}$ versus MBD). MBD-guided repair walks in 429/640 episodes versus 408/640 for phase-aware gradients (38 MBD-only, 17 gradient-only; $p = 0.0065$). True sensor selection reaches 451/640 (Table 1). Against phase deviation, paired walking favors MBD by 202 to 21 ($p = 2.5 \times 10^{-38}$); gated and ungated deviation give identical repair outcomes. Screened

Table 1: Results across three embodiments. For Go2, R^2 measures action prediction on 16 clean trajectories, and Diagnosed reports top-1 sensor identification across 37 faults. Go2 Walk and Survive are counts over 640 episodes. Online MBD detects, diagnoses, and repairs faults within each episode. Go1 and ANYmal C report walking over 352 episodes per method. On these two robots, the GBM predicts actions directly and shares neither MBD's gait model nor its input representation.

	Go2				Walk	
Method	R^2	Diagnosed	Walk	Survive	Go1	ANYmal C
No repair	–	–	259	373	197	162
MBD + PRR	0.9766	27	**429**	467	305	265
Online MBD + PRR	–	–	382	419	–	–
GBM–TreeSHAP + PRR	0.9764	5	277	361	266	239
Phase-aware gradient + PRR	–	**33**	408	455	319	283
Phase deviation + PRR	–	8	248	361	–	–
Ground-truth sensor + PRR	–	37	451	494	–	–

faults show larger gains (92/288 to 219/288 over nine repaired types) than the other eleven (167/352 to 210/352). The overall gain is 26.6 percentage points (exploratory 95% fault-cluster bootstrap interval 11.7–41.7; 20,000 resamples), conditional on suite selection.

Despite similar clean-action R^2 (0.9764 versus 0.9766), matched GBM–TreeSHAP identifies 5/37 faults and walks in 277/640 episodes, not significantly above no repair ($p = 0.076$) and below MBD ($p = 1.2 \times 10^{-33}$). Reused faults and differing masks limit attribution-specific conclusions.

Online operation and anchor-contact faults. Online MBD + PRR raises walking from 259/640 to 382/640 (128 gains, 5 losses; $p = 6.1 \times 10^{-32}$). It triggers in 454/640 faulty episodes, at median step 274 ($5.48\,\mathrm{s}$ from episode start, among triggers), and in 0/64 held-out fault-free episodes (Wilson 95% upper bound 5.7%). Faults are injected from the first step, and step 274 is the earliest permitted decision; 444 of the 454 triggers occur there. The fault-free set includes noise and pushes: 35/64 walk, including all 16 clean, unpushed episodes. A deviation detector counts readings beyond two healthy phase-conditioned standard deviations. Its threshold is the maximum one-second outlier fraction over the same calibration episodes. It never triggers and leaves walking at 259/640; other thresholds and detectors remain untested. For three front-left anchor-contact faults, PRR walks in 71/96 episodes versus 76/96 without repair ($p = 0.18$); healthy counterparts walk in 75/96. These faults do not reduce aggregate walking on this block, and repair adds no benefit.

Other embodiments. Separate fits on Go1 and ANYmal C test 13 shared faults at $0.5\,\mathrm{m/s}$. Their gait and phase-modulated feedback are fitted jointly, without Go2's clipping or alternating-control data. Separate healthy screens select push magnitudes. Repair tests 11 non-anchor faults with/without push: 352 episodes per robot. MBD diagnoses 6/13 and 8/13 faults, respectively, and improves walking on both (Table 1). Phase-aware gradients reach 602/704 versus MBD's 570/704 (42 gradient-only, 10 MBD-only; $p = 9.1 \times 10^{-6}$). Go2's method ranking does not transfer.

4 Discussion and Conclusion

MBD is the central diagnostic contribution, while PRR provides a controlled way to test whether its diagnoses support effective intervention. The structured decomposition makes the surrogate's sensor contributions traceable without claiming to reveal the frozen policy's internal mechanism. A matched boosted-tree surrogate achieves similar clean-action accuracy but does not provide comparable diagnostic or repair performance. Clean-action accuracy alone is therefore insufficient evidence of diagnostic value. Our evidence is limited to one policy in simulation, a partly screened fault suite, separately fitted surrogates for each robot, and simulator-derived references. Future work should evaluate independently specified faults, cross-robot transfer, robust phase estimation, abstention, simultaneous faults, and onboard latency. Extension to manipulation and vision–language–action policies also remains open.

References

[1] Open X-Embodiment Collaboration. Open X-Embodiment: Robotic learning datasets and RT-X models. In *IEEE International Conference on Robotics and Automation*, 2024.

[2] M. J. Kim, K. Pertsch, S. Karamcheti, T. Xiao, A. Balakrishna, S. Nair, R. Rafailov, E. Foster, G. Lam, P. Sanketi, Q. Vuong, T. Kollar, B. Burchfiel, R. Tedrake, D. Sadigh, S. Levine, P. Liang, and C. Finn. OpenVLA: An open-source vision-language-action model. In *Conference on Robot Learning*, 2024.

[3] N. Bohlinger, G. Czechmanowski, M. Krupka, P. Kicki, K. Walas, J. Peters, and D. Tateo. One policy to run them all: an end-to-end learning approach to multi-embodiment locomotion. In *Conference on Robot Learning*, 2024.

[4] R. Isermann. Model-based fault-detection and diagnosis – status and applications. *Annual Reviews in Control*, 29(1):71–85, 2005.

[5] A. Shrikumar, P. Greenside, and A. Kundaje. Learning important features through propagating activation differences. In *International Conference on Machine Learning*, pages 3145–3153, 2017.

[6] M. Sundararajan, A. Taly, and Q. Yan. Axiomatic attribution for deep networks. In *International Conference on Machine Learning*, pages 3319–3328, 2017.

[7] B. Häon, K. C. Stocking, I. Chuang, and C. Tomlin. Mechanistic interpretability for steering vision-language-action models. In *Conference on Robot Learning*, 2025. URL https://openreview.net/forum?id=YvsUD8C9QS.

[8] H. Buurmeijer, C. Amo Alonso, A. Swann, and M. Pavone. Observing and controlling features in vision-language-action models, 2026. URL https://arxiv.org/abs/2603.05487.

[9] Z. Ravichandran, A. Robey, V. Kumar, G. J. Pappas, and H. Hassani. Safety guardrails for LLM-enabled robots. *IEEE Robotics and Automation Letters*, 11(4):4649–4656, 2026. doi:10.1109/LRA.2026.3667488.

[10] S. Peri, B. Pandit, C. Kim, F. Li, and S. Lee. Simple masked training strategies yield control policies that are robust to sensor failure. In *Proceedings of the Conference on Robot Learning*, volume 270 of *Proceedings of Machine Learning Research*, pages 4463–4482, 2024.

[11] F. Acero and Z. Li. Distilling reinforcement learning policies for interpretable robot locomotion: Gradient boosting machines and symbolic regression. In *2024 IEEE/RSJ International Conference on Intelligent Robots and Systems*, pages 6840–6847, 2024. doi:10.1109/IROS58592.2024.10802433.

[12] A. Srisuchinnawong and P. Manoonpong. Growable and interpretable neural control with online continual learning for autonomous lifelong locomotion learning machines. arXiv:2505.12029, 2025.

[13] M. Vincze, L. Ferrarotti, L. L. Custode, B. Lepri, and G. Iacca. SMoSE: Sparse mixture of shallow experts for interpretable reinforcement learning in continuous control tasks. In *Proceedings of the AAAI Conference on Artificial Intelligence*, volume 39, pages 20982–20990, 2025. doi:10.1609/aaai.v39i20.35394.

[14] K. Stocking and B. Häon. The case for physical AI safety. Physical AI Safety Institute white paper, July 2026. URL https://www.paisi.ai/the-case-for-physical-ai-safety.

[15] S. Ross, G. Gordon, and D. Bagnell. A reduction of imitation learning and structured prediction to no-regret online learning. In *Proceedings of the Fourteenth International Conference on Artificial Intelligence and Statistics*, pages 627–635, 2011.

[16] J. H. Friedman. Greedy function approximation: A gradient boosting machine. *The Annals of Statistics*, 29(5):1189–1232, 2001.

[17] S. M. Lundberg, G. Erion, H. Chen, A. DeGrave, J. M. Prutkin, B. Nair, R. Katz, J. Himmelfarb, N. Bansal, and S.-I. Lee. From local explanations to global understanding with explainable AI for trees. *Nature Machine Intelligence*, 2(1):56–67, 2020.